Variable-Temperature ^{87}Rb Magic-Angle Spinning NMR Spectroscopy of Inorganic Rubidium Salts

Jørgen Skibsted and Hans J. Jakobsen*

Instrument Centre for Solid-State NMR Spectroscopy, Department of Chemistry, University of Aarhus, DK-8000 Aarhus C, Denmark

Received: April 20, 1999; In Final Form: August 6, 1999

Temperature dependencies of the ^{87}Rb quadrupole coupling constants (C_Q), asymmetry parameters (η_Q), and isotropic chemical shifts (δ_{iso}) have been observed and determined for RbCl, $RbClO_4$, Rb_2SO_4, and $RbNO_3$ from variable-temperature (VT) ^{87}Rb magic-angle spinning (MAS) NMR spectra for the temperature range from about −100 to +165 °C. VT ^{87}Rb multiple-quantum MAS NMR spectra of the trigonal form for $RbNO_3$ have assisted the retrival of C_Q, η_Q, and δ_{iso} for the three Rb sites of this phase. The results demonstrate that $C_Q(^{87}Rb)$ and $\delta_{iso}(^{87}Rb)$ are highly temperature-dependent for all samples over the studied temperature range. Linear correlations of δ_{iso} with temperature, corresponding to temperature coefficients in the range −0.014 to −0.036 ppm/°C (i.e., increasing shielding with increasing temperature), are observed for all samples. An exception is the Rb(2) site in Rb_2SO_4 for which a small linear decrease in shielding is observed with increasing temperature. For $RbClO_4$ and Rb_2SO_4 the three $C_Q(^{87}Rb)$ values decrease linearly with negative temperature coefficients in the range −7.0 to −1.6 kHz/°C. Linear correlations are observed for the two η_Q values for Rb_2SO_4, while η_Q decreases parabolically with increasing temperature for $RbClO_4$. The C_Q and η_Q parameters for $RbNO_3$ exhibit nonmonotonic variations with temperature. These variations are ascribed to an increase in molecular motions (displacements/reorientations) for the NO_3 groups with temperature. For $RbClO_4$, Rb_2SO_4, and $RbNO_3$ the dependencies of the principal elements of the quadrupole tensors on temperature are evaluated and relationships between these dependencies and variations of structural parameters associated with thermal expansion of the unit cells are discussed. The observed dependencies of C_Q, η_Q, and δ_{iso} on temperature may account for the generally minor discrepancies in these parameters reported in the literature for $RbClO_4$, Rb_2SO_4, and $RbNO_3$ from NMR experiments at ambient temperatures.

Introduction

High-resolution solid-state NMR spectroscopy of half-integer spin quadrupolar nuclei has become an important tool in the structural characterization of inorganic compounds, of metal complexes, and for a wide variety of technologically important materials including molecular sieves, cements, ceramics, minerals, glasses, and catalysts. This is mainly due to the introduction of a number of improved and different sample-spinning and rf-pulse techniques in recent years. These greatly aid in the exploitation of the quadrupolar interaction, which strongly depends on the local electronic structure and geometry at the nuclear site. In the development of these techniques, inorganic rubidium salts such as $RbClO_4$, Rb_2SO_4, and $RbNO_3$ have often been chosen for the preliminary demonstrations of the experiments. For example, $RbClO_4$ and Rb_2SO_4 have been used as model compounds for static-powder,[1,2] single-crystal,[3] and magic-angle spinning (MAS)[4,5] NMR methods in exploring the combined effect of quadrupole coupling and chemical shielding anisotropy from ^{87}Rb NMR spectra. Most recently, the eight parameters required to characterize the effects of the two interactions on ^{87}Rb NMR spectra have been obtained for $RbClO_4$ and Rb_2SO_4 from the more sophisticated and technically demanding techniques of three-dimensional dynamic-angle correlation spectroscopy (DACSY)[6] and the two-dimensional (2D) switched-angle spinning (SAS) experiment.[7] Furthermore, $RbNO_3$ has been extensively employed in dynamic-angle spinning (DAS) NMR[8−10] and multiple-quantum (MQ) MAS NMR[10−13] to demonstrate the removal of the second-order quadrupole line shape for the three distinct Rb sites in $RbNO_3$ in one dimension of the 2D NMR spectra. The second dimension of these spectra displays separate second-order quadrupolar line shapes for the three sites, which allow a determination of the quadrupole coupling parameters (C_Q and η_Q). However, a comparison of the reported values for C_Q, η_Q, and the isotropic chemical shifts (δ_{iso}) for the rubidium salts shows some discrepancies that cannot be attributed to the particular experiments and/or simulations.

This work presents a variable-temperature (VT) ^{87}Rb MAS NMR study of RbCl, $RbClO_4$, Rb_2SO_4, and $RbNO_3$ over a temperature range from about −100 to +165 °C. The results demonstrate that C_Q, η_Q, and δ_{iso} for these compounds are highly temperature-dependent in this temperature range. Thus, the variations observed for the parameters in the literature may at least partly be ascribed to slightly different sample temperatures for the different studies. Differences in sample temperatures for experiments performed at ambient temperature may, for example, originate from the frictional heating induced by sample spinning,[14] since sample temperatures up to approximately 60 °C have been observed for large rotors at high spinning speeds.

^{87}Rb VT NMR has earlier been used in studies of the ferroelectric−paraelectric phase transition for RbH_2AsO_4[15] and RbH_2PO_4,[16] the incommensurate phases of Rb_2ZnCl_4[17] and Rb_2-

* To whom correspondence should be addressed. Phone: +45 8942 3842. Fax: +45 8616 6199. E-mail: hja@kemi.aau.dk.

10.1021/jp9912861 CCC: $18.00
Published on Web 09/23/1999

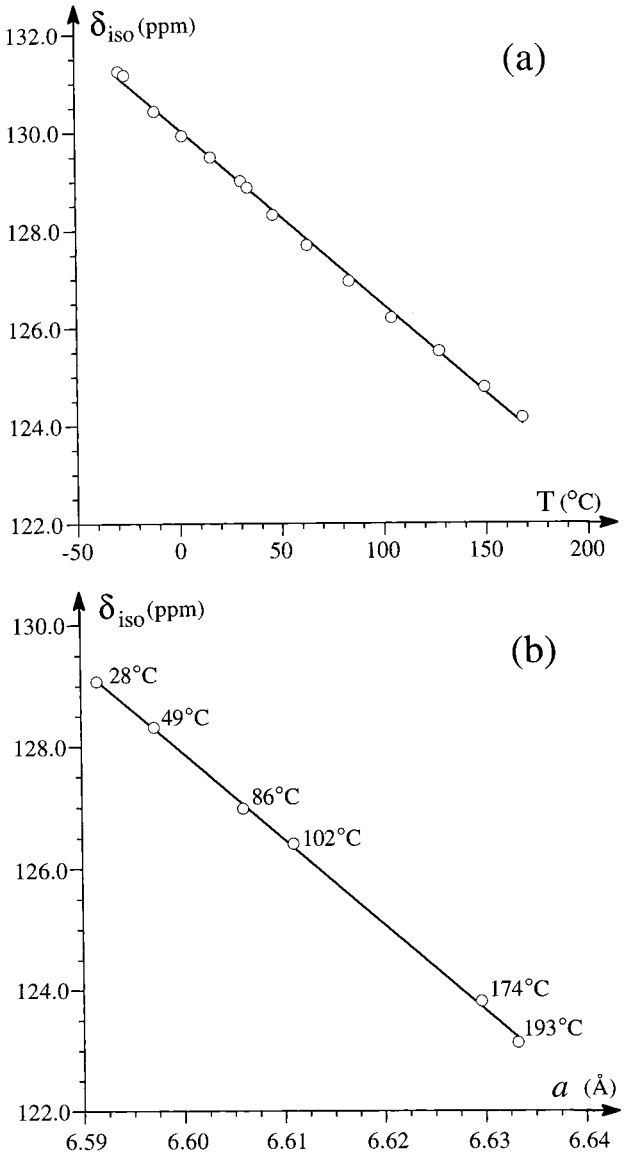

Figure 1. Linear correlations between ^{87}Rb isotropic chemical shifts (δ_{iso}) for RbCl and (a) temperature (T) and (b) the lattice constant (a) for the cubic unit cell at six different temperatures. The lattice constants for RbCl are taken from ref 32, and the corresponding δ_{iso} values at these temperatures are calculated from eq 1.

$ZnBr_4$,[18] the antiferroelectric−paraelectric phase transition for RbSCN [19] and of the second-order structural phase transition (tetragonal-cubic) that occurs in the perovskite-type crystals $RbCaF_3$[20] and $Rb_xK_{1-x}MnF_3$.[21] Generally, these studies have investigated the temperature dependence of the quadrupolar interaction and/or the spin−lattice relaxation time employing ^{87}Rb single-crystal NMR. In most cases only a single, fixed, and well-defined orientation of the crystal in the magnetic field was investigated, utilizing the fact that the point symmetries of the Rb sites in the crystals imply axially symmetric electric-field gradient (EFG) tensors. From early investigations of the temperature dependence of nuclear quadrupole resonance frequencies,[22] it is predicted that C_Q decreases with increasing temperature for ionic solids, considering the effects from the lattice expansion and the increase in amplitude of the thermal vibrations. In agreement with this prediction, decreasing ^{87}Rb quadrupole couplings with increasing temperatures are reported for the tetragonal form of $RbCaF_3$[20] and for the monoclinic phase II of $RbNO_2$.[23] However, for the paraelectric phases of RbH_2AsO_4 and RbH_2PO_4, an anomalous increase in $C_Q(^{87}Rb)$ with increasing temperature is observed and ascribed to result from atomic motions.[15,16]

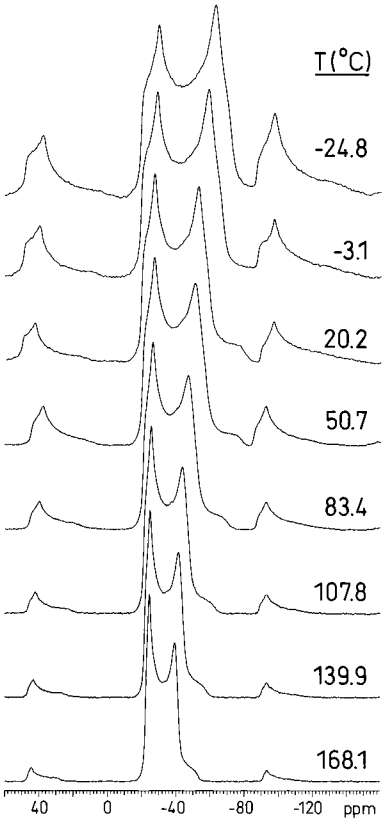

Figure 2. ^{87}Rb VT MAS NMR spectra (7.1 T) of the central transition for $RbClO_4$ obtained for the temperature range from −24.8 to +168.1 °C using a spinning speed of 6.6 ± 0.1 kHz.

The above-mentioned ^{87}Rb NMR studies have not considered the temperature dependence for the ^{87}Rb isotropic chemical shifts. However, variations in isotropic chemical shifts with temperature have earlier been investigated for several diamagnetic inorganic solids, including ^{81}Br and ^{127}I NMR of alkali metal halides,[24] ^{205}Tl chemical shifts for thallium salts,[25] and ^{63}Cu, ^{35}Cl, ^{81}Br, and ^{127}I chemical shifts for cuprous halides.[26] In these studies the isotropic chemical shifts were observed to vary linearly with temperature. A deshielding with increasing temperature was observed for the anions and for ^{205}Tl, while the ^{63}Cu chemical shielding increased with increasing temperature for the cuprous halides. By means of a simple theory for the chemical shielding, these temperature variations have been related to lattice expansion and thermal-vibration-induced changes of the overlap integrals for the bonding orbitals.[24] More recently, the strong temperature dependence of the ^{207}Pb chemical shift for $Pb(NO_3)_2$ has been investigated with the aim of using this sample as a chemical shift thermometer in MAS NMR studies.[27]

Experimental Section

Samples of RbCl, $RbClO_4$, Rb_2SO_4, and $RbNO_3$ were purchased from Alfa Products and used without further purification. Since an irreversible phase transition may occur for $RbNO_3$ at 73 °C,[28] the sample of $RbNO_3$ was recrystallized from an aqueous solution at room temperature. The crystal structure and phase purity of all rubidium samples were checked by powder X-ray diffraction prior to the NMR studies. ^{87}Rb MAS NMR spectra were recorded on Varian INOVA-300 (7.1 T) and

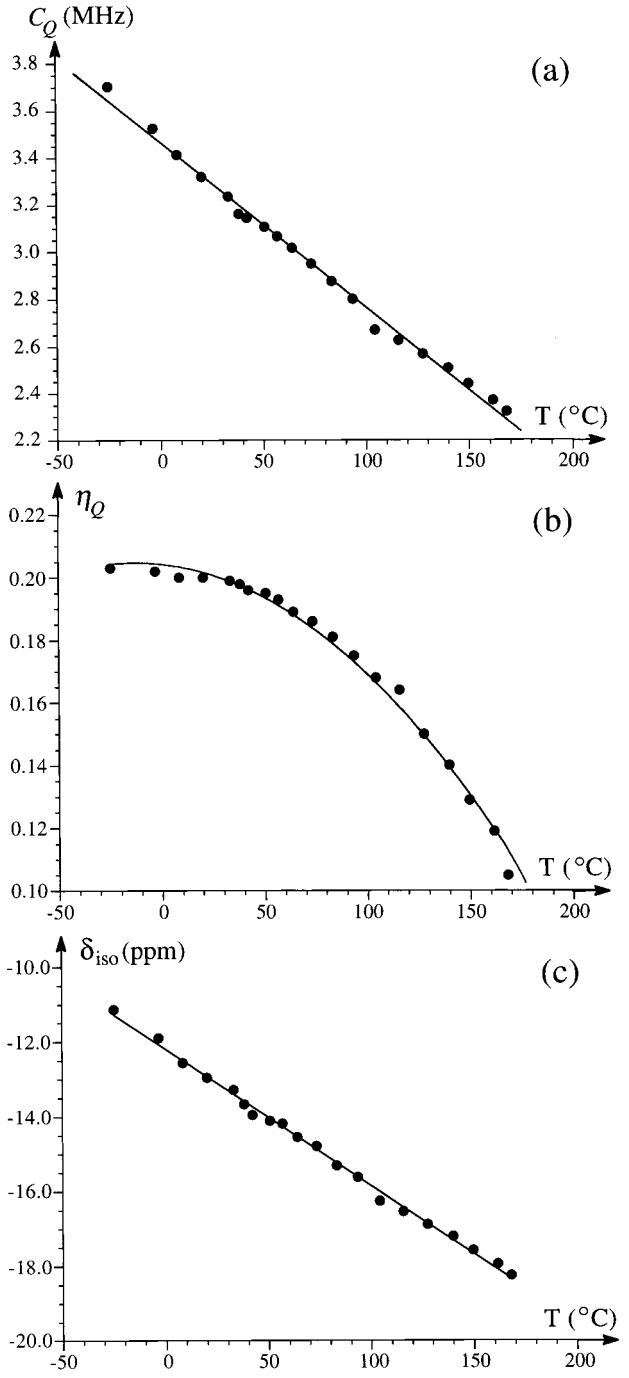

Figure 3. Graphs illustrating the temperature dependencies for ^{87}Rb C_Q (a), η_Q (b), and δ_{iso} (c) in $RbClO_4$ over the temperature range from −24.8 to +168.1 °C. The straight lines (a and c) and the curve (b) correspond to the result from regression analyses given by eqs 3−5 for parts a−c, respectively.

INOVA-400 (9.4 T) spectrometers using home-built narrow-bore 7 and 4 mm VT cross polarization (CP) MAS NMR probes, respectively. Both probes employ dry drive gas at ambient temperature at the cone of drive jets and dry hot−cold (N_2) gas that is split at the air bearings of the stator and the sample. The probes are capable of operating in the temperature range from approximately −150 to +250 °C. Temperature regulation (±1 °C) is performed using a home-built temperature controller−heater system based on a commercial microprocessor for temperature regulation. The temperature gradient over the rotor volume is less than 2 °C. The actual sample temperature was determined using ^{207}Pb MAS NMR of $Pb(NO_3)_2$ as a NMR thermometer.[27] A slice of $Pb(NO_3)_2$ was packed below the sample at the buttom of the rotor, and the ^{87}Rb and ^{207}Pb MAS NMR spectra were recorded under identical conditions. For some experiments, an additional slice of $NaNO_3$ was packed at the top of the rotor to allow for exact setting of the magic angle by minimization of the line widths observed for the spinning sidebands from the ^{23}Na satellite transitions.

Single-pulse ^{87}Rb experiments at 7.1 T (7 mm probe) were performed employing pulse widths of 1 μs ($RbClO_4$ and $RbNO_3$) and 4 μs (RbCl) for $\gamma B_1/(2\pi) = 47$ kHz, spinning speeds of 6−7 kHz, and relaxation delays of 1 s ($RbClO_4$ and $RbNO_3$) and 4 s (RbCl). Phase-sensitive ^{87}Rb MQMAS spectra for $RbNO_3$ (7.1 T) were obtained employing the basic two-pulse

TABLE 1: ^{87}Rb Quadrupole Coupling Constants (C_Q), Asymmetry Parameters (η_Q), and Isotropic Chemical Shifts (δ_{iso}) for $RbClO_4$ at Five Selected Temperatures[a]

T (°C)	C_Q (MHz)	η_Q	δ_{iso} (ppm)
−24.8	3.704	0.203	−11.13
20.2	3.319	0.200	−12.95
83.3	2.875	0.181	−15.31
139.9	2.506	0.140	−17.20
168.1	2.322	0.105	−18.25

[a] Estimated error limits are ±0.005 MHz for C_Q, ±0.005 for η_Q, and ±0.2 ppm for δ_{iso}, while the temperature is measured with an accuracy of ±1 °C.

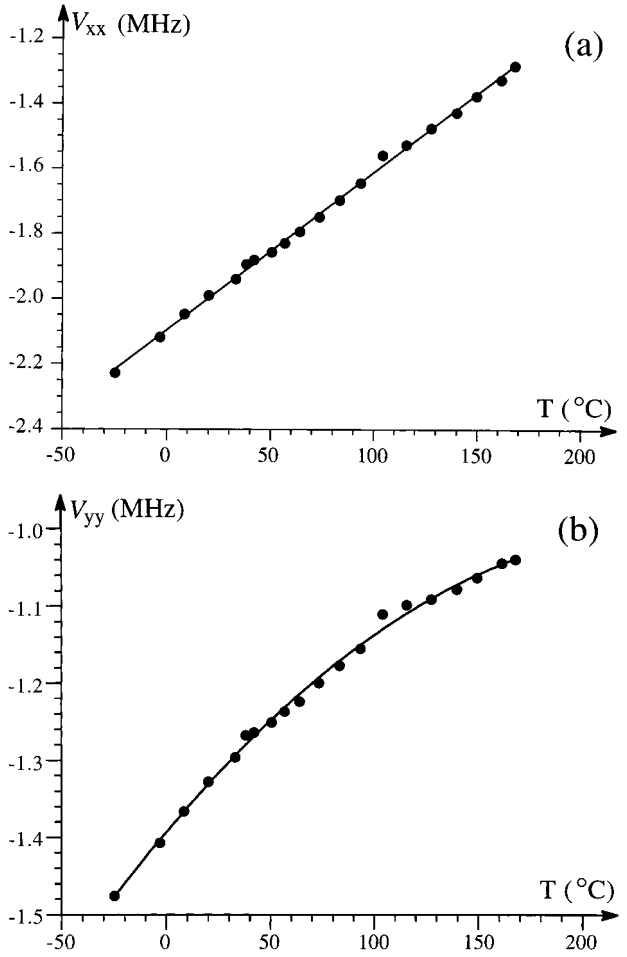

Figure 4. Plots of the ^{87}Rb principal elements $V_{xx} = (-1/2)C_Q(\eta_Q + 1)$ (a) and $V_{yy} = (1/2)C_Q(\eta_Q - 1)$ (b) of the quadrupole coupling tensor versus temperature for $RbClO_4$ assuming a positive value for the quadrupole coupling constant (i.e., the V_{zz} element). The results from the least-squares analysis of the data in parts a and b are given in eqs 6 and 7, respectively.

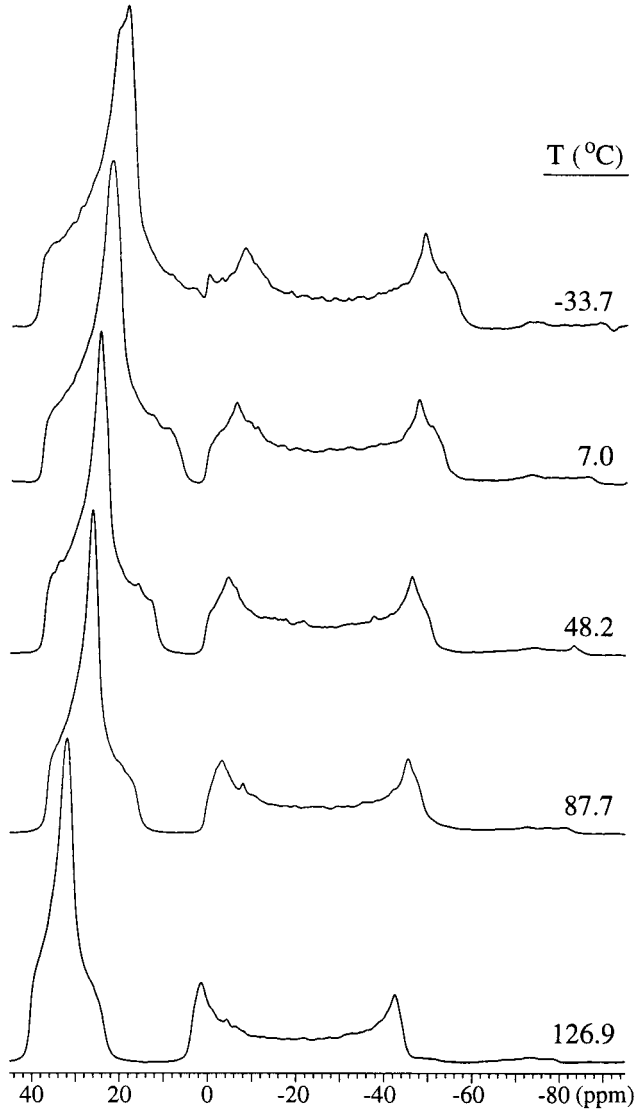

Figure 5. ^{87}Rb MAS NMR spectra (9.4 T) of the central transitions for Rb_2SO_4 obtained for the temperature range from −33.7 to +126.9 °C using a spinning speed of about 13 kHz.

TABLE 2: ^{87}Rb Quadrupole Coupling Constants (C_Q), Asymmetry Parameters (η_Q), and Isotropic Chemical Shifts (δ_{iso}) for Rb_2SO_4 at Five Selected Temperatures[a]

	Rb(1)			Rb(2)		
T (°C)	C_Q (MHz)	η_Q	δ_{iso} (ppm)	C_Q (MHz)	η_Q	δ_{iso} (ppm)
−33.7	3.05	0.89	42.52	5.42	0.160	15.67
7.0	2.75	0.95	41.81	5.34	0.121	15.86
48.2	2.45	0.99	41.40	5.27	0.096	16.11
87.7	2.22	0.96	40.84	5.22	0.066	16.50
126.9	1.99	0.90	40.21	5.15	0.040	16.83

[a] Estimated error limits are ±0.01 MHz for C_Q and ±0.2 ppm for δ_{iso} for both sites. For Rb(1) and Rb(2) the error limits for η_Q are ±0.01 and ±0.005, respectively. The temperature is measured with an accuracy of ±1 °C.

sequence,[29] a 36-step phase cycle,[30] and a pulse width of 21.2 μs (i.e., 360° liquid pulse) for both pulses. The spectra were recorded with spinning speeds of 6−7 kHz, a t_1 increment of 50 μs, and a total of 128 increments. For each increment, 108 scans were typically acquired with a repetition delay of 0.5 s, resulting in an experiment time of about 2 h. The single-pulse experiments at 9.4 T (4 mm probe) for Rb_2SO_4 were obtained using a pulse width of 1 μs ($\gamma B_1/(2\pi) = 58$ kHz), spinning speeds between 12.6 and 13.8 kHz, and a relaxation delay of 1 s. Isotropic chemical shifts are relative to a 1.0 M aqueous solution of RbCl at 20 °C. Simulations, least-squares fitting, and numerical error analysis were performed on a SUN SPARC 5 workstation using the STARS solid-state NMR software package, developed in our laboratory[4,31] and presently available as a part of the Varian VNMR software.

TABLE 3: Results of the Linear Regression Analysis for the Temperature Dependencies of the ^{87}Rb Quadrupole Couplings and Isotropic Chemical Shifts ($X = AT + B$) for Rb_2SO_4[a]

	parameter (X)	slope (A)[b]	interscept (B)[c]
Rb(1)	δ_{iso}	−0.0136	41.98
	η_Q (T < 60 °C)	1.13×10^{-3}	0.936
	η_Q (T > 60 °C)	-1.64×10^{-3}	1.12
	C_Q	-6.50×10^{-3}	2.79
	V_{33}[d]	-6.98×10^{-3}	2.79
	V_{22}[d]	1.47×10^{-3}	−0.09
	V_{11}[d]	5.51×10^{-3}	−2.70
Rb(2)	δ_{iso}	0.0072	15.87
	η_Q	0.734×10^{-3}	0.13
	C_Q (V_{zz})	-1.55×10^{-3}	5.35
	V_{yy}	-1.24×10^{-3}	−2.33
	V_{xx}	2.79×10^{-3}	−3.02

[a] The analyses include data from 15 ^{87}Rb MAS NMR spectra and give linear correlation coefficients $R > 0.98$ in all cases. A positive value for V_{zz} is assumed in the calculation of V_{xx}, V_{yy}, and V_{zz}. [b] Slope in units of ppm/°C for δ_{iso}, (°C)$^{-1}$ for η_Q, and MHz/°C for C_Q, V_{xx}, V_{yy}, and V_{zz}. [c] Interscept in units of ppm for δ_{iso} and in MHz for C_Q, V_{xx}, and V_{yy}. [d] The principal elements of the quadrupole tensor are defined as $V_{33} = V_{zz}$, $V_{22} = V_{yy}$, and $V_{11} = V_{xx}$ below 60 °C and as $V_{33} = V_{xx}$, $V_{22} = V_{yy}$, and $V_{11} = V_{zz}$ for temperatures above 60 °C.

Results and Discussion

Previous ^{87}Rb NMR investigations of $RbClO_4$ and Rb_2SO_4[1−5] have shown that ^{87}Rb in these salts possesses a small chemical shielding anisotropy (CSA) with a span ($\Omega = |\delta_{11} - \delta_{33}|$) Ω < 44 ppm.[3] The ^{87}Rb VT MAS NMR spectra in this work are recorded using high spinning speeds ($6 < \nu_r < 13$ kHz) at moderate magnetic fields (7.1 and 9.4 T) under which conditions the CSA is efficiently averaged by MAS. Thus, the CSA interaction is not considered in the simulations. The results of the ^{87}Rb VT MAS NMR are discussed below in order of increasing complexity for the experimental spectra.

RbCl. Rubidium chloride has a cubic structure ($Fm\bar{3}m$),[32] implying that the ^{87}Rb site in RbCl should not possess any quadrupole coupling. In agreement with this fact and earlier studies,[1,8,33] the present ^{87}Rb MAS NMR spectra of RbCl display a single narrow resonance from the ^{87}Rb central transition; however, spinning sidebands are also observed over a spectral range of about 150 kHz. These originate from the satellite transitions for ^{87}Rb sites, affected by point defects and/or strain in the crystallites, similar to the observation for the ^{79}Br MAS NMR spectrum of KBr.[34] ^{87}Rb VT MAS NMR spectra of RbCl (not shown), covering a temperature range from −28 to +168 °C, reveal the temperature dependencies of δ_{iso}(^{87}Rb) shown in Figure 1a. As seen from this graph, δ_{iso} decreases linearly with increasing temperature (T), and a regression analysis gives

$$\delta_{iso} = (-0.0361 \text{ ppm/°C})T + 130.09 \text{ ppm} \qquad (1)$$

with a correlation coefficient $R = 0.99$. Thermal expansion for RbCl has earlier been investigated by X-ray diffraction for six temperatures in the range +28 to +193 °C.[32] Figure 1b illustrates that calculated δ_{iso} values (from eq 1) correlate with

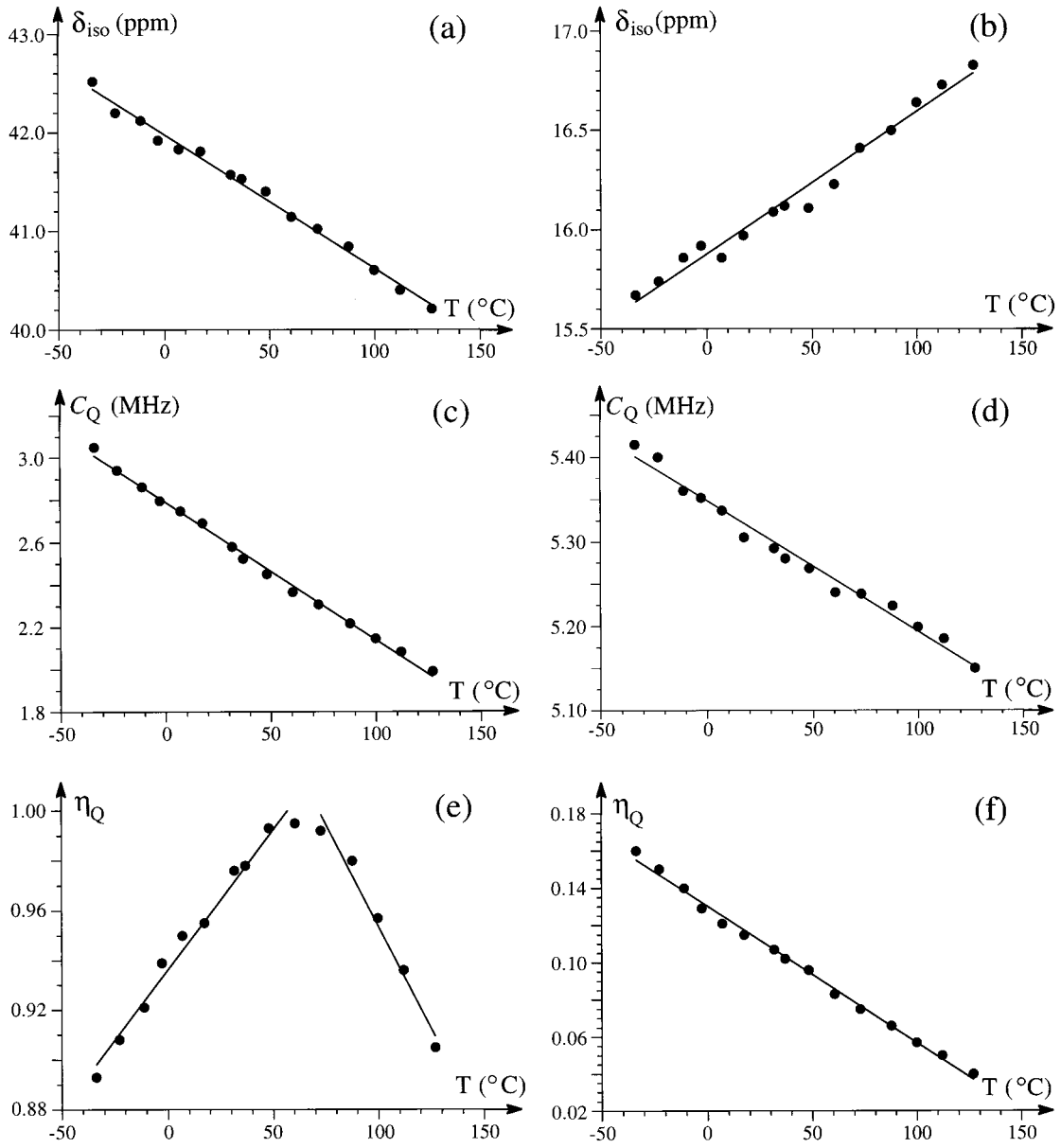

Figure 6. Temperature dependencies for the ^{87}Rb isotropic chemical shifts (a, b), quadrupole coupling constants (c, d), and asymmetry parameters (e, f) for Rb_2SO_4 over the temperature range from −33.7 to +126.9 °C. The plots in parts a, c, and e correspond to the Rb(1) site and those in parts b, d, and f to Rb(2). The results of the linear regression analyses are illustrated by the straight lines, and the corresponding regression equations are summarized in Table 3.

the lattice constant (a) of the cubic unit cell[32] for these temperatures according to

$$\delta_{iso} = (-141.1 \text{ ppm/Å})a + 1061.19 \text{ ppm} \quad (R = 0.99) \quad (2)$$

The observation of a linear dependence of δ_{iso} with temperature is in agreement with earlier VT studies of the chemical shift for the cations ^{205}Tl and ^{63}Cu in thallium salts and cuprous halides, respectively.[25,26] Using simple theory for the chemical shielding of a nucleus and considering only its nearest-neighbor ions, Ngai[24] has calculated the effect from the temperature dependence of the mean overlap integral for the bonding orbitals and found that the contribution from thermal vibrational motions to $d\delta/dT$ is opposite in sign to the dilatation effect caused by lattice expansion. According to this model, increased shielding with increasing temperature may be observed in cases where the dilatation effect dominates over the contribution from thermal vibrational motions as observed experimentally for ^{87}Rb in RbCl (eq 1). From the model of Ngai and the observed temperature dependence of δ_{iso}, it also seems plausible that δ_{iso} should exhibit a correlation with the lattice constant of the unit cell as actually also observed in Figure 1b.

$RbClO_4$. ^{87}Rb VT MAS NMR spectra illustrating the central transition for $RbClO_4$ over a temperature range from −25 to +168 °C are shown in Figure 2. The spectra are obtained using a spinning speed of about 6.0 kHz, which allows observation of the centerband from the central transition without overlap from the first-order spinning sidebands for temperatures above 20 °C. From the line shape of the centerbands, it is apparent that the ^{87}Rb quadrupole coupling constant decreases significantly while the asymmetry parameter decreases slightly with increasing temperature. Evidence for a decrease of $C_Q(^{87}Rb)$ with an increase in temperature has earlier been obtained from frictional heating caused by MAS.[4] Least-squares fitting of simulated line shapes to the experimental line shapes for the

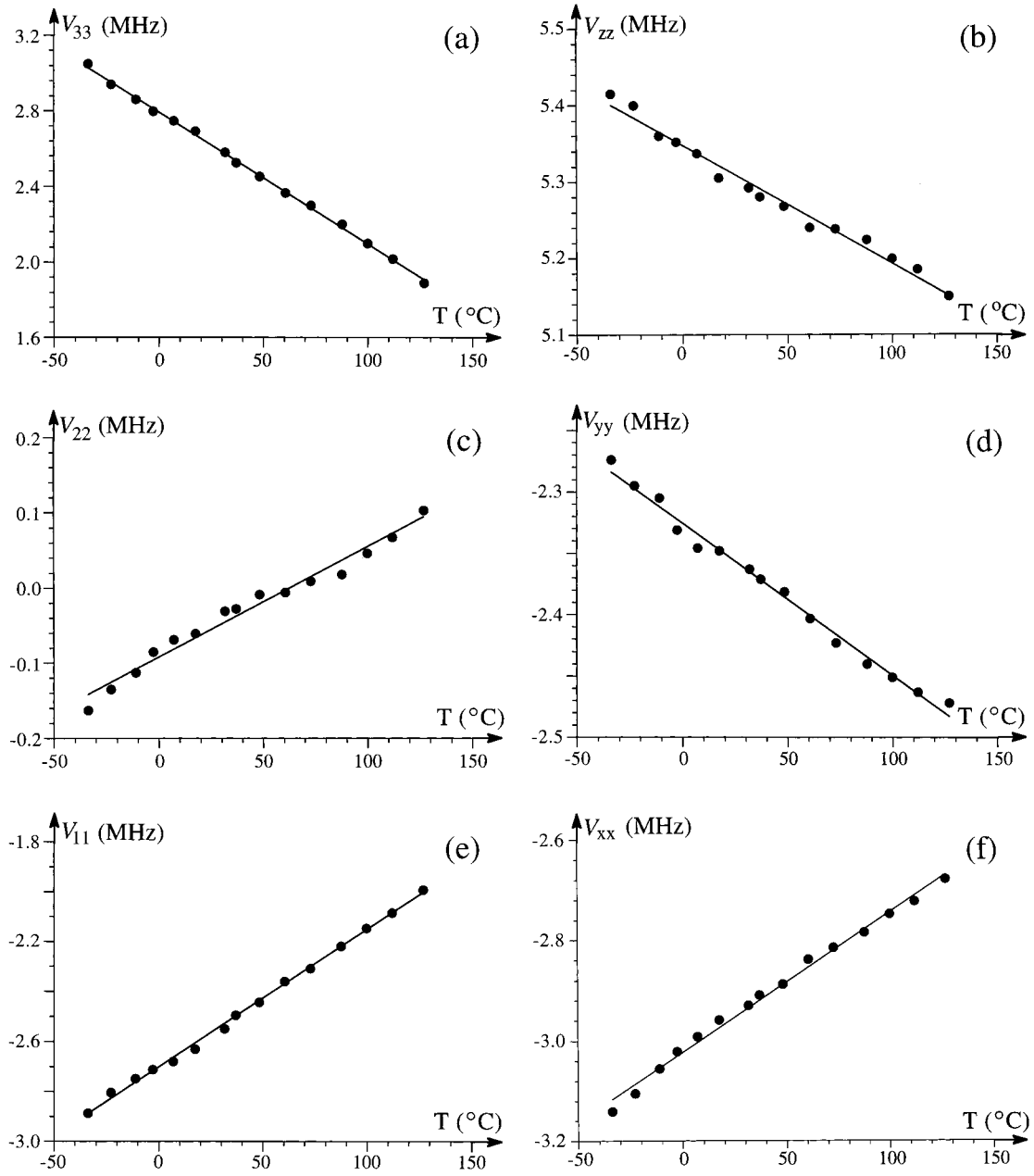

Figure 7. Plots of the principal elements of the quadrupole tensor as a function of temperature for the Rb(1) (a, c, e) and Rb(2) (b, d, f) in Rb_2SO_4. The V_{ii} elements for Rb(1) are defined as $V_{33} = V_{zz}$, $V_{22} = V_{yy}$, and $V_{11} = V_{xx}$ for $T < 60$ °C and as $V_{33} = V_{xx}$, $V_{22} = V_{yy}$, and $V_{11} = V_{zz}$ for $T > 60$ °C. The results from a linear regression analysis are illustrated by the straight lines, and the corresponding regression equations are summarized in Table 3.

centerband and first-order spinning sidebands, observed for 20 ^{87}Rb MAS spectra over the temperature range from −25 to +168 °C, reveal the C_Q, η_Q, and δ_{iso} values shown as a function of temperature in Figure 3a−c and given in Table 1 for five selected temperatures. A linear correlation between C_Q and temperature given by

$$C_Q = (-7.04 \times 10^{-3}\ \text{MHz/°C})T + 3.47\ \text{MHz} \quad (R = 0.997) \quad (3)$$

is obtained from the data in Figure 3a. Figure 3b displays a monotonic decrease of η_Q with increasing temperature, which may be fitted to a second-order polynomial according to

$$\eta_Q = (-2.80 \times 10^{-6}\ °\text{C}^{-2})T^2 - (7.21 \times 10^{-5}\ °\text{C}^{-1})T + 0.204 \quad (4)$$

with $R = 0.995$. Quadrupole coupling parameters in the range 3.19 MHz $\le C_Q \le$ 3.30 MHz and $0.10 \le \eta_Q \le 0.21$ have earlier been reported for $RbClO_4$ from ^{87}Rb NMR at ambient temperatures.[1−4,8] By use of the temperature dependence of C_Q (eq 3) as a thermometer, this range of C_Q values corresponds to sample temperatures from 24 to 40 °C. Temperatures in this range can occur as a result of frictional heating induced by the sample spinning[14] and/or by the heat generated by excessive current in the room-temperature shim coils. Thus, slight variations in the sample temperatures may account for the deviations in quadrupole couplings reported for $RbClO_4$.

A linear correlation between δ_{iso} and temperature is also observed for $RbClO_4$ (Figure 3c). Regression analysis gives

$$\delta_{iso} = (-0.0365\ \text{ppm/°C})T + 12.18\ \text{ppm} \quad (R = 0.998) \quad (5)$$

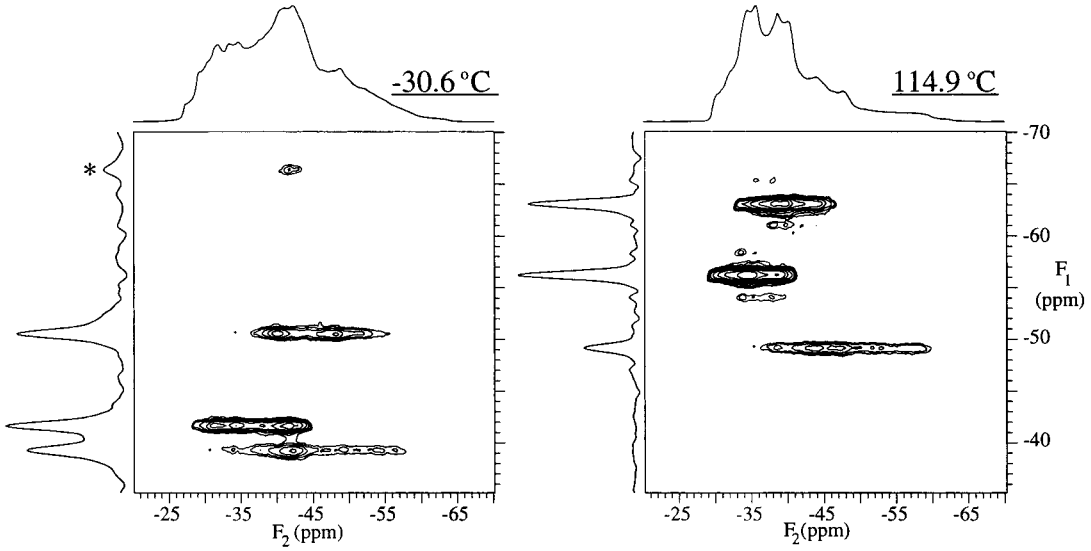

Figure 8. Contour plots of ^{87}Rb MQMAS NMR spectra (7.1 T) of $RbNO_3$ at −30.6 and 114.9 °C, obtained using spinning speeds of 6.1 and 6.6 kHz, respectively, and shown on identical scales in the F_1 and F_2 dimensions. The scales for both dimensions are referenced to a 1.0 M aqueous solution of RbCl at 20 °C. The projections onto the isotropic (F_1) dimension correspond to summations over the 2D spectra, while the ^{87}Rb MAS NMR spectra, obtained at the same temperatures, are shown at the top of the 2D plots. The asterisk in the spectrum recorded at −30.6 °C indicates a spinning sideband originating from the resonance for Rb(2) at $\delta_{3Q}^{exp} = -39.3$ ppm.

TABLE 4: ^{87}Rb Quadrupole Coupling Constants (C_Q), Asymmetry Parameters (η_Q), and Isotropic Chemical Shifts (δ_{Iso}) for the Three Rb Sites in Trigonal $RbNO_3$ at Selected Temperatures[a]

	Rb(1)			Rb(2)			Rb(3)		
T (°C)	C_Q (MHz)	η_Q	δ_{iso} (ppm)	C_Q (MHz)	η_Q	δ_{iso} (ppm)	C_Q (MHz)	η_Q	δ_{iso} (ppm)
−101.7	2.60	0.34	−30.41	2.29	0.72	−24.45	2.37	0.30	−24.22
−48.4	2.28	0.40	−30.99	2.15	0.86	−26.09	2.13	0.22	−25.38
−30.6	2.18	0.41	−31.23	2.11	0.90	−26.79	2.07	0.20	−25.93
0.3	1.96	0.46	−31.65	2.02	0.97	−27.88	1.88	0.15	−26.89
10.6	1.88	0.47	−31.78	2.01	0.96	−28.24	1.84	0.16	−27.18
29.3	1.77	0.54	−32.03	2.01	0.90	−28.90	1.72	0.19	−27.59
38.1	1.72	0.56	−32.10	2.02	0.87	−28.99	1.69	0.22	−27.72
46.4	1.67	0.58	−32.16	2.03	0.85	−29.32	1.64	0.25	−27.91
55.1	1.64	0.58	−32.25	2.04	0.82	−29.43	1.59	0.30	−28.17
93.6	1.44	0.67	−32.97	2.10	0.77	−30.70	1.37	0.63	−29.07
114.9	1.37	0.72	−33.37	2.12	0.76	−30.89	1.29	0.75	−29.49
137.8	1.27	0.80	−33.74	2.13	0.76	−31.17	1.21	0.88	−30.19
149.7	1.22	0.84	−34.17	2.15	0.76	−31.47	1.18	0.90	−30.73

[a] Tentative assignment of the quadrupole coupling parameters to the three structural sites given in ref 28 (see text). Estimated error limits for C_Q are ±0.01 MHz for Rb(1) and Rb(3) and ±0.02 MHz for Rb(2). For η_Q and δ_{iso} the error limits are estimated to ±0.02 and ±0.3 ppm for all sites. The temperature is measured with an accuracy of ±1 °C.

The increase in shielding with increasing temperature (i.e., $d\delta/dT < 0$) is almost identical for $RbClO_4$ and RbCl (eq 1). This indicates that lattice expansion also has a dominating influence on $d\delta/dT$ for $RbClO_4$.

A more appropriate approach for evaluation of the temperature dependencies of C_Q and η_Q is through calculation of the principal elements for the quadrupole coupling tensor. In units of MHz these are given by $V_{zz} = C_Q$, $V_{yy} = (^1/_2)C_Q(\eta_Q - 1)$, and $V_{xx} = (-^1/_2)C_Q(\eta_Q + 1)$ using the convention $|V_{zz}| \geq |V_{xx}| \geq |V_{yy}|$. Assuming a positive value for the principal element of the EFG tensor (V_{zz}), these relations give the temperature dependencies for V_{xx} and V_{yy} illustrated in Figure 4a and b, respectively (Figure 3a shows the variation with temperature for V_{zz}). Figure 4a reveals a linear correlation between V_{xx} and temperature according to

$$V_{xx} = (4.84 \times 10^{-3}\ \text{MHz/°C})T - 2.10\ \text{MHz} \quad (R = 0.999) \quad (6)$$

while the variation for V_{yy} with temperature may be correlated to a second-order polynomial corresponding to the equation

$$V_{yy} = (-6.53 \times 10^{-6}\ \text{MHz °C}^{-2})T^2 + (3.21 \times 10^{-3}\ \text{MHz °C}^{-1})T - 1.39\ \text{MHz} \quad (7)$$

with $R = 0.998$. $RbClO_4$ has an orthorhombic crystal structure (*Pnma*)[35] with the Rb atoms situated in a mirror plane. From a ^{87}Rb single-crystal NMR study of $RbClO_4$ at ambient temperature,[3] it is known that the V_{xx} element of the ^{87}Rb quadrupole coupling tensor is perpendicular to the mirror plane and parallel to the crystallographic *b* axis, while the V_{yy} and V_{zz} elements are in the mirror plane rotated 27° relative to the *a* and *c* axes. It is noteworthy that the quadrupole coupling tensor element (V_{yy}), which does not exhibit a linear temperature dependence, is situated as one of the two elements in the mirror plane.

In agreement with earlier experimental results[20,23] for ^{87}Rb in $RbCaF_3$ and $RbNO_2$, we observe a decrease in quadrupole coupling with increasing temperature, which may result from lattice dilatation and an increase in amplitude of thermal vibrations according to theoretical considerations.[22] Although,

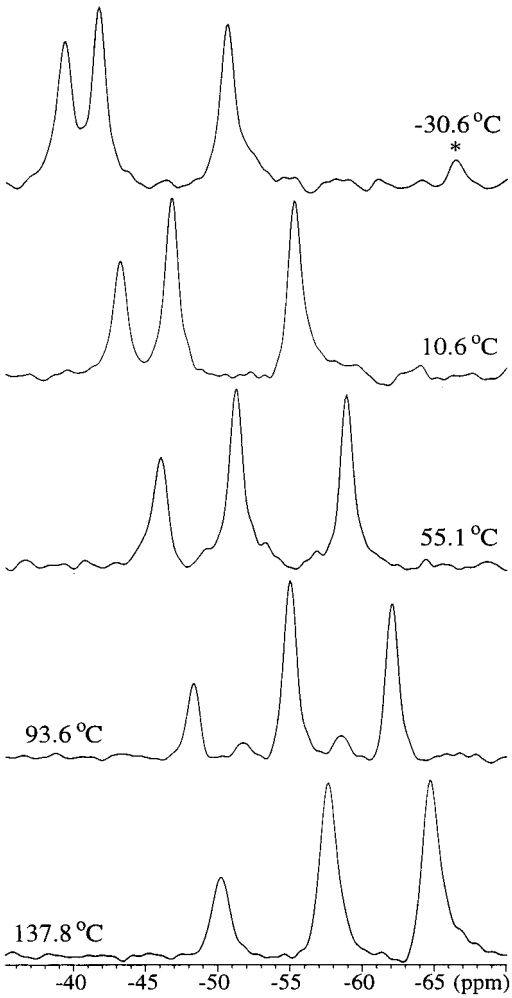

Figure 9. Isotropic projections from ^{87}Rb MQMAS NMR spectra (7.1 T, $\nu_r = 6.1-6.7$ kHz) of $RbNO_3$ at selected temperatures in the range from −30.6 to +137.8 °C. The spectra are obtained as summations over the resonances in the 2D spectra and are referenced to a 1.0 M aqueous solution of RbCl at 20 °C. The asterisk indicates a spinning sideband originating from the resonance for Rb(2) at $\delta_{3Q}^{exp} = -39.3$ ppm.

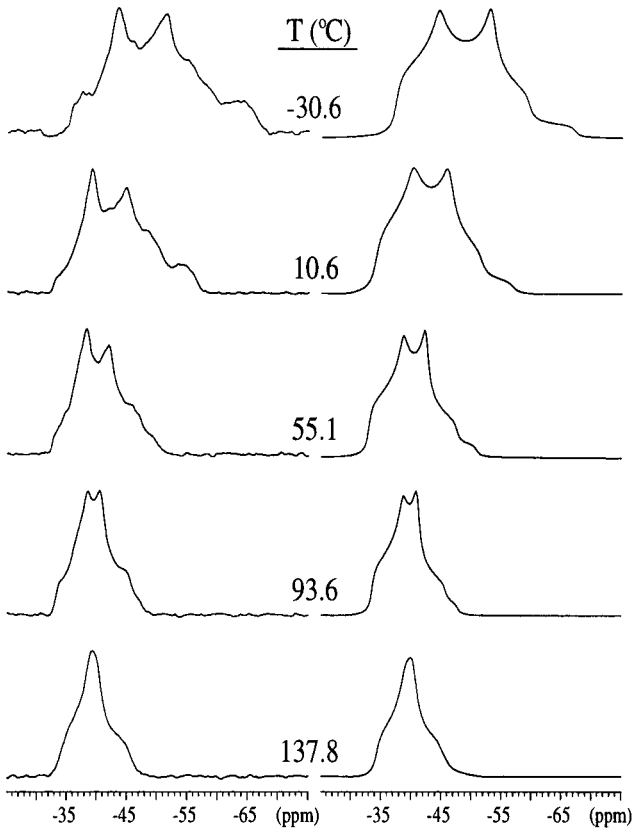

Figure 10. Anisotropic projections from ^{87}Rb MQMAS NMR spectra (7.1 T, $\nu_r = 6.1-6.7$ kHz) of $RbNO_3$ for the Rb(1) site at selected temperatures in the range from −30.6 to +137.8 °C (left column) obtained by summation over the resonance for the Rb(1) site in the 2D spectra. The right-hand column of spectra illustrate optimized simulations of the experimental quadrupolar line shapes for Rb(1). The corresponding parameters for this site are listed in Table 4.

TABLE 5: Results of the Linear Regression Analysis for the Temperature Dependencies of the ^{87}Rb Isotropic Chemical Shifts ($\delta_{iso} = AT + B$) for Trigonal $RbNO_3$[a]

	slope (A) (ppm/°C)	interscept (B) (ppm)	R
Rb(1)	−0.0142	−31.67	0.991
Rb(2)	−0.0290	−27.70	0.992
Rb(3)	−0.0249	−26.76	0.998

[a] The analyses include data obtained from simulation of 23 ^{87}Rb MAS NMR spectra covering a temperature range from −101.7 to 149.7 °C.

a VT crystallographic investigation has not been reported for $RbClO_4$, the effect of lattice dilatation has been examined for $RbClO_4$ by calculation of the electric-field gradient (EFG) tensor elements using a point-charge model,[36] which should be a valid approximation for an ionic crystal. The calculations consider only the 12 nearest oxygen atoms surrounding the Rb^+ ion, employ ideal oxygen charges, and assume that the fractional coordinates for $RbClO_4$ (obtained from XRD at room temperature)[35] are temperature-independent. For an isotropic thermal expansion (i.e., the three crystallographic axes increase linearly with identical temperature coefficients) these calculations show a linear decrease in C_Q with increasing temperature and a constant asymmetry parameter, corresponding to an identical value for $|dV_{ii}/dT|$ for the three principal elements. A linear decrease of the numerical values for the three principal elements is also obtained in cases of anisotropic thermal expansion where the crystallographic axes increase linearly with temperature but with different temperature coefficients. These types of expansion also result in linear relationships between η_Q and the temperature. Comparison of the calculations and the experimental results for $RbClO_4$ (Figures 3 and 4) indicates that lattice dilatation alone cannot account for the temperature dependencies of the V_{ii} elements (e.g., thermal vibrations have a marked influence) and/or the thermal expansion of the crystals is accompanied by a rearrangement of the atomic positions within the unit cell (e.g., such as a rotation of the ClO_4^- ions). Thus, our results proposes the performance of a VT X-ray investigation for $RbClO_4$ in order to gain further information about the lattice dilatation and the atomic rearrangements with temperature.

Rb_2SO_4. Selected ^{87}Rb VT MAS NMR spectra of the central transitions for Rb_2SO_4 covering the temperature range from −34 to +127 °C are shown in Figure 5. The spectra exhibit two centerband resonances with an intensity ratio of 1:1, in agreement with previous ^{87}Rb NMR studies[1,3,5] and the reported crystal structure from single-crystal X-ray diffraction.[37] In our recent ^{87}Rb single-crystal NMR study of Rb_2SO_4,[3] the resonances corresponding to the small and large quadrupole coupling were assigned to the structural Rb(1) and Rb(2) sites,[37] respectively. From the VT MAS spectra in Figure 5, it is apparent that the C_Q values for both sites decrease with

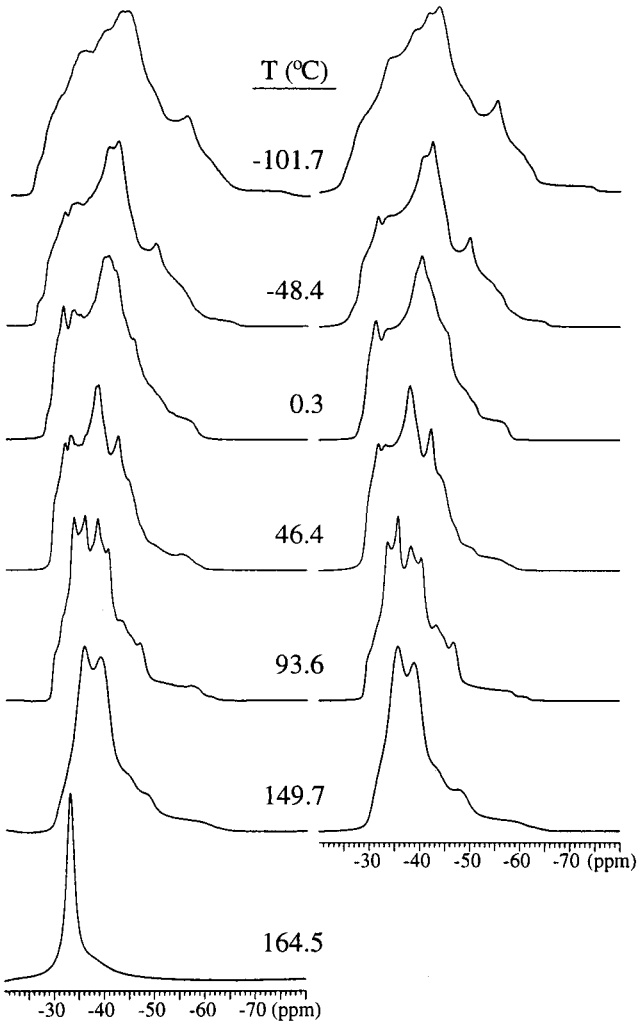

Figure 11. ^{87}Rb MAS NMR spectra (left column) and simulations (right column) of the central transition for $RbNO_3$ at selected temperatures in the range from −101.7 to +164.5 °C. The experimental spectra are obtained at 7.1 T using spinning speeds in the range from 5.6 to 6.8 kHz. The spectrum at 164.5 °C shows a single sharp resonance for the cubic phase of $RbNO_3$ (see text), while the spectra at lower temperatures correspond to the trigonal phase of $RbNO_3$. The simulations employed the optimized C_Q, η_Q, and δ_{iso} parameters for the three Rb sites in the trigonal phase of $RbNO_3$ listed in Table 4.

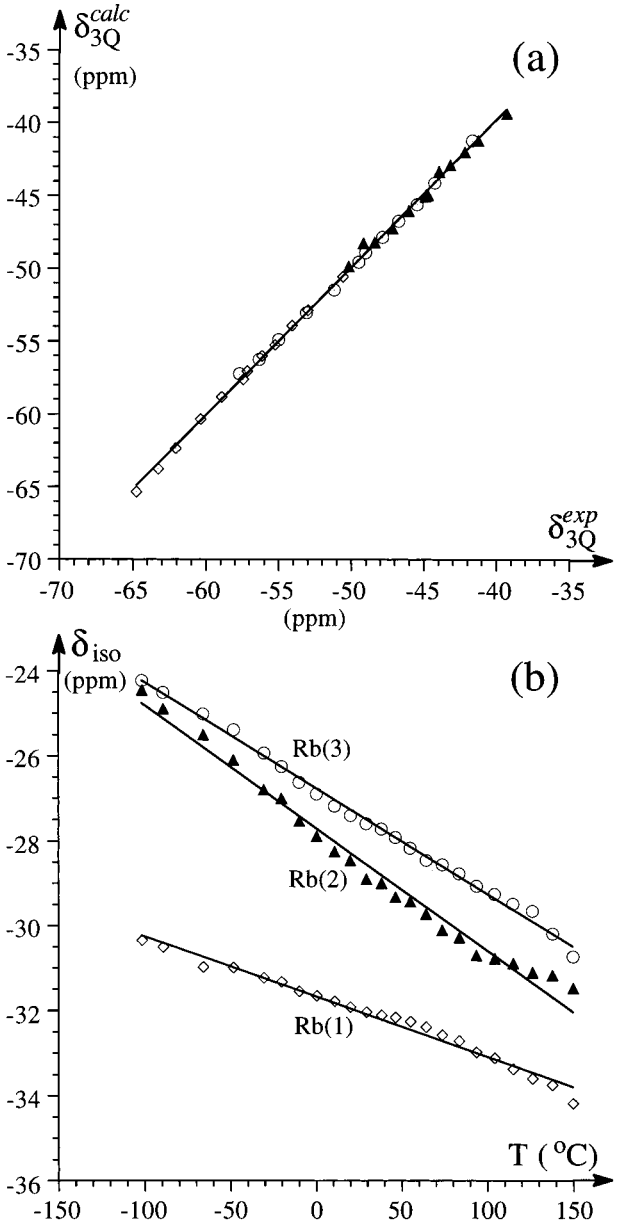

Figure 12. (a) Correlation between calculated (δ_{3Q}^{calc}) and experimental (δ_{3Q}^{exp}) isotropic 3Q shifts for $RbNO_3$ obtained from 12 ^{87}Rb MQMAS NMR spectra (7.1 T) in the temperature range from −30.6 to +137.8 °C. The calculated 3Q shifts are obtained using eq 8 and the C_Q, η_Q, and δ_{iso} values for $RbNO_3$ listed in Table 4. The straight line corresponds to a 1:1 correlation. (b) Temperature dependencies of the ^{87}Rb isotropic chemical shifts for the three Rb sites in $RbNO_3$ over a temperature range from −101.7 to +149.7 °C. The results from linear regression analysis are illustrated by the straight lines, and the corresponding regression equations are summarized in Table 5. In parts a and b the diamonds correspond to the Rb(1) site, solid triangles to Rb(2), and open circles to the Rb(3) site.

increasing temperature and that η_Q decrease slightly for Rb(2) with increasing temperature. Simulations of the centerband line shapes, observed in 15 ^{87}Rb MAS NMR spectra, result in the C_Q, η_Q, and δ_{iso} values for the two Rb sites shown as a function of temperature in Figure 6 and given in Table 2 for the spectra in Figure 5.

A linear correlation between δ_{iso} and temperature is observed for Rb(1) and correspond to an increase in shielding with increasing temperature. The numerical value of the temperature coefficient for δ_{iso} (cf. Table 3) is somewhat smaller than the values observed for RbCl and $RbClO_4$ (eqs 1 and 5). For Rb(2), in contrast, δ_{iso} changes only by 1.2 ppm over the studied temperature range and exhibits a linear correlation with temperature corresponding to a deshielding with increasing temperature. According to the theoretical work of Ngai,[24] this significant difference in temperature dependence of δ_{iso} for Rb(1) and Rb(2) may reflect lattice dilatation on δ_{iso} dominating over the contribution from thermal vibrational motions for Rb(1), while the opposite holds for Rb(2). Further information about the relationship of these temperature dependencies and lattice dilatation calls for a VT crystallographic investigation on Rb_2SO_4.

Linear relationships between C_Q and the temperature is observed for both sites (Figure 6c and d) where the result from regression analysis (Table 3) reveals a factor of 4 larger temperature coefficient for Rb(1) compared to Rb(2). The temperature coefficient for Rb(1) is similar to the value determined for $RbClO_4$ (eq 3). The asymmetry parameter for Rb(2) decreases linearly with the temperature over the studied temperature range (Figure 6f), while η_Q increases for Rb(1) with

TABLE 6: Results of the Least-Squares Analysis for the Temperature Dependencies of the Principal Elements of the ^{87}Rb Quadrupole Coupling Tensors for Trigonal $RbNO_3$ Employing Up to Fourth-Order Polynomials ($V_{ii} = a_4T^4 + a_3T^3 + a_2T^2 + a_1T + a_0$)[a]

		$a_4 \times 10^{-10}$ MHz (°C)$^{-4}$	$a_3 \times 10^{-8}$ MHz (°C)$^{-3}$	$a_2 \times 10^{-5}$ MHz (°C)$^{-2}$	$a_1 \times 10^{-3}$ MHz (°C)$^{-1}$	a_0 MHz
Rb(1)	V_{zz} (C_Q)				−5.62	1.99
	V_{yy}			−0.292	3.27	−0.52
	V_{xx}			−0.396	2.72	−1.44
Rb(2)	V_{33}[b]	−5.43	10.5	1.32	−3.16	1.99
	V_{22}[b]	2.40	−7.25	−0.731	3.54	0.01
	V_{11}[b]	2.96	−3.13	−0.571	−0.371	−2.00
Rb(3)	V_{zz} (C_Q)				−5.03	1.88
	V_{yy}	−15.9	6.74	4.26	2.33	−0.80
	V_{xx}	13.2	−10.3	−3.53	3.06	−1.10

[a] The analyses include data from simulations of 23 ^{87}Rb MAS NMR spectra covering a temperature range from −101.7 to 149.7 °C. A positive value for C_Q is assumed in the calculation of V_{xx} and V_{yy} for Rb(1) and Rb(3). [b] The principal elements of the quadrupole tensor for Rb(2) are defined as $V_{33} = V_{zz}$ (=C_Q), $V_{22} = V_{yy}$, and $V_{11} = V_{xx}$ for temperatures below −2 °C and as $V_{33} = V_{xx}$, $V_{22} = V_{yy}$, and $V_{11} = V_{zz}$ (=C_Q) for $T > -2$ °C. A positive value of C_Q for $T < -2$ °C is assumed.

increasing temperature in the range −30 to +60 °C (Figure 6e). In contrast, a linear decrease of η_Q with increasing temperature is observed for Rb(1) above 60 °C, which demonstrates that the principal elements of the quadrupole coupling tensor must be redefined at 60 °C according to our definition ($|V_{zz}| \geq |V_{xx}| \geq |V_{yy}|$). This corresponds to a sign reversal for C_Q and V_{yy} at 60 °C. To account for this, we introduce the definition $V_{11} = V_{xx}$, $V_{22} = V_{yy}$, and $V_{33} = V_{zz}$ for the principal elements below 60 °C and $V_{11} = V_{zz}$,$V_{22} = V_{yy}$, and $V_{33} = V_{xx}$ for temperatures above 60 °C. The redefinition results in the temperature dependencies of the individual principal EFG tensor elements shown in Figure 7a,c,e for Rb(1), while the corresponding values for V_{zz}, V_{yy}, and V_{xx} for Rb(2) are shown in Figure 7b,d,f. All principal quadrupole coupling tensor elements exhibit linear correlations with temperature, and the results from a regression analyses are summarized in Table 3. The temperature coefficients for V_{33} and V_{11} for Rb(1) are very similar to the corresponding values for V_{zz} (C_Q) and V_{xx} for $RbClO_4$ (eqs 3 and 6), whereas somewhat smaller numerical values for the coefficients for V_{zz} (C_Q) and V_{xx} for Rb(2) in Rb_2SO_4 are observed. The linear relationships between the principal V_{ii} elements and temperature may indicate that the effect from lattice dilatation on the EFG tensors dominates the contribution from thermal vibrations for Rb_2SO_4.

$RbNO_3$. At ambient temperature and pressure, $RbNO_3$ is trigonal (space group $P3_1$) and contains three Rb sites in the asymmetric unit.[38] When heated, $RbNO_3$ transforms at 164 °C to a cubic CsCl-type structure with a unique Rb site.[39] The three Rb sites for the trigonal form possess similar magnitudes for their quadrupolar interactions and isotropic chemical shifts. Thus, this phase is most often chosen as a suitable test sample to demonstrate the performance of new 2D experiments, as for example DAS and MQMAS,[8−13] for quadrupolar nuclei.

Single-pulse MAS NMR spectra (7.1 T) of the central transitions for trigonal $RbNO_3$ reveal heavily overlapping quadrupolar line shapes from the three Rb sites and thereby prevent a straightforward determination of the quadrupolar coupling parameters. Thus, standard two-pulse MQMAS NMR spectra[12,29] have been recorded in order to unambiguously determine C_Q, η_Q, and δ_{iso} for the three Rb sites. Contour plots of the ^{87}Rb MQMAS NMR spectra at −30.6 and 114.9 °C are shown in Figure 8 and indicate significant changes in C_Q, η_Q, and δ_{iso} for the three sites at these temperatures. This is apparent from the width of the contours in the F_2 dimension and from the isotropic triple-quantum (3Q) shifts (δ_{3Q}) observed in the F_1 dimension. From 12 ^{87}Rb MQMAS spectra, covering the temperature range −30.6 to +137.8 °C, the isotropic 3Q shifts (cf. Figure 9) are found to decrease almost linearly with increasing temperature. Valuable parameters for C_Q, η_Q, and δ_{iso} are obtained from the MQMAS spectra from simulation of partial summations over the individual resonances in the anisotropic (F_2) dimension using second-order quadrupolar line shapes. A tentative assignment of the quadrupole coupling parameters to the three different Rb sites has been obtained from point-charge calculations[36] using the structural data reported from single-crystal X-ray diffraction at 23 and 99 °C.[28] Illustrative F_2 summations over the resonance for the Rb(1) site in the MQMAS spectra are shown in Figure 10 along with optimized simulated quadrupolar line shapes. From these spectra it is apparent that a significant reduction in C_Q and an increase in η_Q occur for Rb(1) with increasing temperature. The agreement between the experimental and simulated quadrupolar line shapes for Rb(1) (Figure 10) is somewhat lower for the spectra at lowest temperatures, which may reflect the fact that the excitation−conversion of 3Q coherences in MQMAS NMR depends strongly upon the magnitude of the quadrupolar interaction.[29,40] Especially strong quadrupolar couplings combined with relatively low rf field strengths (i.e., $\gamma B_1/(2\pi) = 47$ kHz for our 7 mm VT CP-MAS probe) may result in nonideal excitation−conversion profiles and thereby distorted second-order quadrupolar line shapes in the F_2 dimension of the MQMAS spectra.

To improve the precision of C_Q, η_Q, and δ_{iso} for the three Rb sites, the data obtained from the MQMAS spectra have been refined by simulation of single-pulse MAS NMR spectra recorded at the same temperatures. Furthermore, 11 additional MAS NMR spectra have been included in the analysis, resulting in a total of 23 spectra covering the temperature range from −101.7 to +163.5 °C. Selected ^{87}Rb MAS NMR spectra over this temperature range are shown in Figure 11 along with the optimized simulations for which the C_Q, η_Q, and δ_{iso} parameters are summarized in Table 4. The spectrum at 164.5 °C displays a single sharp resonance with the isotropic chemical shift $\delta_{iso} = -33.2 \pm 0.2$ ppm, which agrees with the occurrence of a phase transformation from the trigonal to the cubic phase at 164 °C.[39]

An independent test of the reliability of the C_Q, η_Q, and δ_{iso} values, obtained from the refined simulations of the ^{87}Rb MAS NMR spectra, may be achieved by a comparison of experimental and calculated isotropic 3Q shifts for the MQMAS experiments. For an $I = {}^3/_2$ nulceus, the isotropic 3Q shift (δ_{3Q}^{calc}) is given by the equation[12,29]

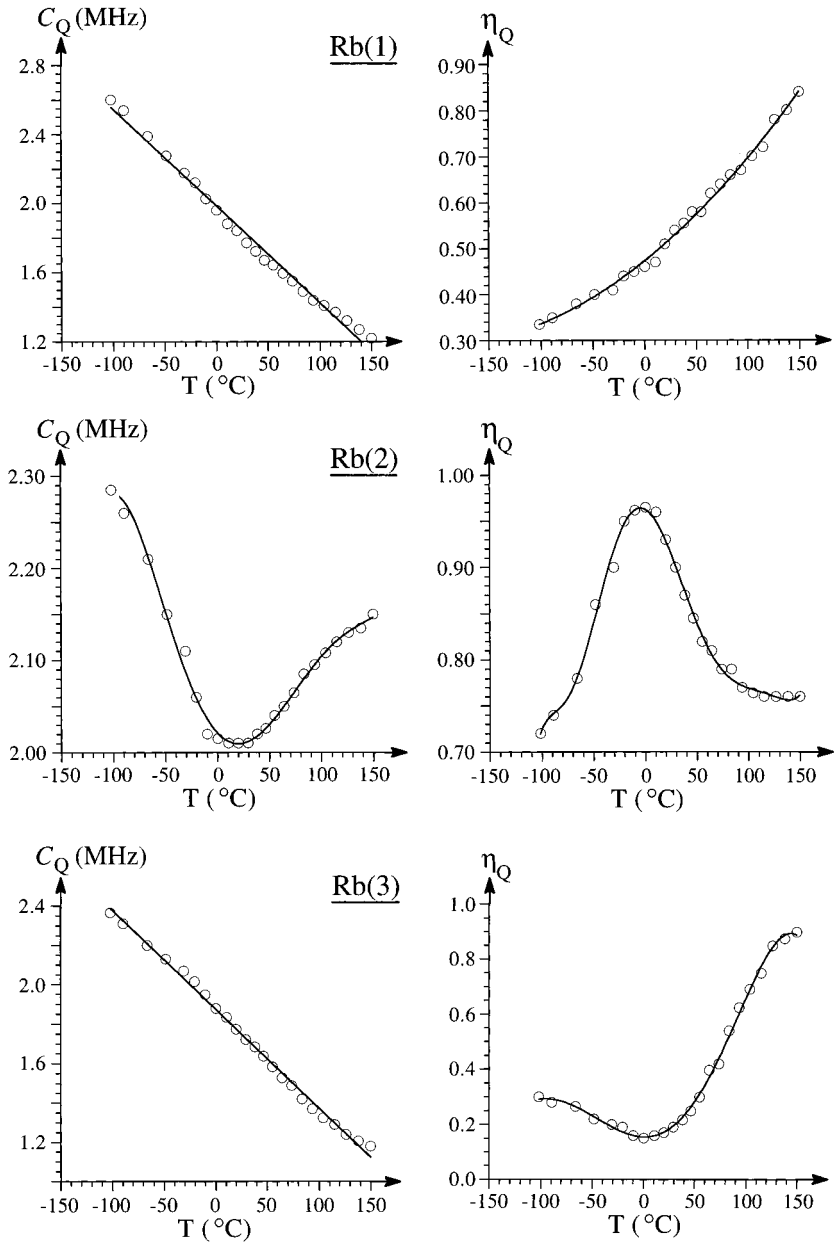

Figure 13. Temperature dependencies of the ^{87}Rb C_Q and η_Q values for the three Rb sites in trigonal $RbNO_3$ over the temperature range from −101.7 to +149.7. The results from regression analysis using up to fourth-order polynomials are illustrated by the solid curves. Linear regression analysis is employed for the C_Q values of the Rb(1) and Rb(2) sites, and the resulting equations are summarized in Table 6.

$$\delta_{3Q}^{calc} = \frac{17}{8}\delta_{iso} + \frac{1}{32}\frac{C_Q{}^2(1+\eta_Q{}^2/3)}{\nu_L{}^2} \times 10^6 \qquad (8)$$

where ν_L is the Larmor frequency. This comparison is illustrated in Figure 12a where calculated isotropic 3Q shifts for the three Rb sites are shown as a function of the experimental values (δ_{3Q}^{exp}) from the 12 MQMAS spectra covering the temperature range −30.6 to +137.8 °C. The straight line in Figure 12a indicates the 1:1 correlation between δ_{3Q}^{calc} and δ_{3Q}^{exp}, and calculation of the mean deviation between δ_{3Q}^{calc} and δ_{3Q}^{exp} for the three Rb sites at the 12 different temperatures gives the value 0.29 ppm. Thus, the refined C_Q, η_Q, and δ_{iso} values from the ^{87}Rb MAS NMR spectra are in excellent agreement with the experimental 3Q shifts, observed in the ^{87}Rb MQMAS spectra.

The overall best agreement of the C_Q, η_Q, and δ_{iso} parameters for $RbNO_3$ determined in this work with those reported earlier from ^{87}Rb DAS and MQMAS NMR spectra,[8,9,12] obtained at ambient temperatures, is observed for the data reported by Massiot et al.[12] from a ^{87}Rb MQMAS NMR study at 7.1 T when compared to the present values at 38.1 °C in Table 4. However, neither of the reported sets of data agree exactly with our parameters for a specific temperature in the range 10−50 °C. Of the parameters C_Q, η_Q, and δ_{iso}, we expect that the quadrupole coupling constants are the most precisely determined parameter, especially for Rb(1) and Rb(3), which possess the smallest quadrupole couplings. Using the C_Q values for Rb(1) and Rb(3) as thermometers gives sample temperatures of 38, ∼15, and 45 °C for the experiments reported in refs 12, 8, and 9, respectively, when the quadrupole couplings for Rb(1) and Rb(3) in these studies are compared with those determined in this work. Although care should be excercised in such a comparison because of the error limits for C_Q, these sample temperatures may certainly occur in sample-spinning experiments performed at ambient temperatures as a result of frictional heating−cooling from Joule−Thompson expansion, or heating by the room-temperature shim coils. Thus, the deviations in

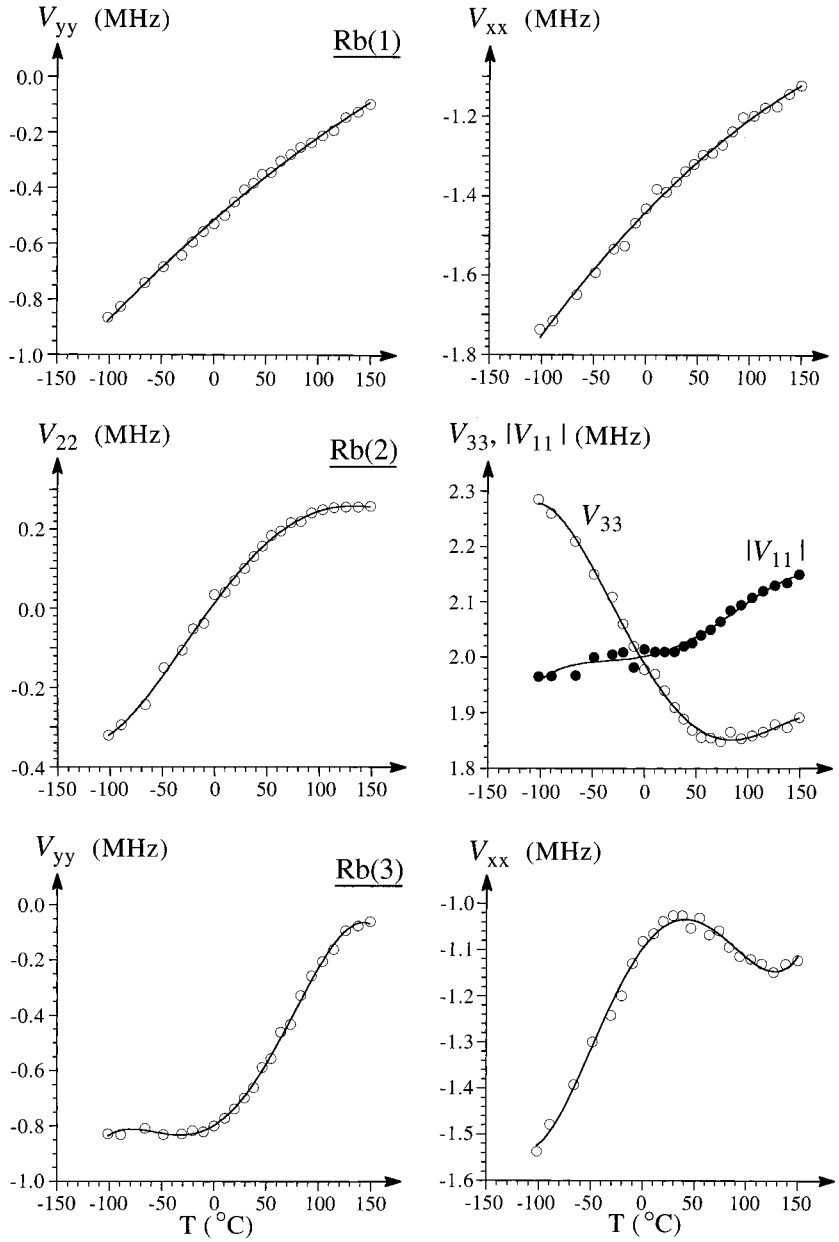

Figure 14. Plots of the principal elements for the quadrupole coupling tensors as a function of temperature for the three Rb sites in trigonal $RbNO_3$. For Rb(1) and Rb(3) the elements V_{yy} and V_{xx} are shown as a function of temperature, whereas for Rb(2) the elements V_{11}, V_{22}, and V_{33} are shown because of the change in sign for C_Q at −2 °C for this site. These elements are defined as $V_{33} = V_{zz}$, $V_{22} = V_{yy}$, and $V_{11} = V_{xx}$ for $T < -2$ °C and as $V_{33} = V_{xx}$, $V_{22} = V_{yy}$, and $V_{11} = V_{zz}$ for $T > -2$ °C. The results from regression analysis using up to fourth-order polynomials are illustrated by the solid curves. The corresponding equations are summarized in Table 6.

quadrupole coupling parameters reported in the literature may originate from minor variations in the actual temperatures of the studied samples of $RbNO_3$.

The temperature dependencies of the isotropic chemical shifts for the three Rb sites in $RbNO_3$ are illustrated in Figure 12b over the temperature range −101.7 to +149.7 °C. The variation of δ_{iso} with temperature can for all three sites best be approximated by linear correlations, corresponding to an increase in shielding with increasing temperature. The results of the linear regression analyses are summarized in Table 5. The Rb(1) site exhibits the smallest temperature coefficient (−0.0142 ppm/°C) and Rb(2) the largest (−0.0290 ppm/°C), i.e., values between the temperature coefficients observed for the Rb(1) site of Rb_2SO_4 and the Rb sites of RbCl and $RbClO_4$. Again, the increase in shielding observed for all three sites in $RbNO_3$ most likely reflects the effects from thermal expansion of the unit cell with increasing temperature.

Figure 13 illustrates the temperature dependencies of the quadrupolar coupling parameters for the Rb sites in $RbNO_3$, which appear to be more complex than those observed for $RbClO_4$ and Rb_2SO_4. For Rb(1) and Rb(3) linear correlations between C_Q and temperature are observed with temperature coefficients (Table 6) similar to those for $RbClO_4$ and the Rb(1) site of Rb_2SO_4. In contrast, the quadrupole coupling constant for Rb(2) exhibits a nonmonotonic behavior over the studied temperature range with a minimum value observed at about 20 °C. Nonmonotonic temperature dependencies are also observed for the asymmetry parameters for Rb(2) and Rb(3), while η_Q increases parabolically with increasing temperature for Rb(1).

Calculation of the principal elements of the quadrupole coupling tensors gives the dependencies for V_{xx} and V_{yy} with temperature shown in Figure 14. The variation of these elements for Rb(2) indicates that the numerical value of the V_{yy} element becomes larger than V_{zz} at −2 °C and thus that a change in

sign of C_Q occurs at this temperature. To account for this, we have introduced the definition $V_{11} = V_{xx}$, $V_{22} = V_{yy}$, and $V_{33} = V_{zz}$ for the principal elements below −2 °C and $V_{11} = V_{zz}$,$V_{22} = V_{yy}$, and $V_{33} = V_{xx}$ for temperatures above −2 °C. Simulation of the rather complex temperature dependencies of the principal quadrupole tensor elements in Figure 14 requires the use of fourth-order polynomials for Rb(2) and Rb(3), while the V_{xx} and V_{yy} elements for Rb(1) may be simulated using second-order polynomials. The results from least-squares analysis of the data in Figure 14 and of the C_Q values for Rb(1) and Rb(3) are summarized in Table 6. The quite unique variations of the individual quadrupole tensor elements with temperature hardly result from a isotropic thermal expansion of the unit cell for trigonal $RbNO_3$.

Pohl et al.[28] have studied trigonal $RbNO_3$ by single-crystal X-ray diffraction and reported the unit cell parameters at four temperatures in the range 23−164 °C and the complete crystal structures at 23 and 99 °C. The thermal expansion coefficients for the *a* and *c* axes of the trigonal unit cell are very similar, and a plot of *a* and *c* versus temperature shows that these lattice constants increase parabolically with increasing temperature. Furthermore, Pohl et al.[28] reported that an irreversible first-order phase transition occurs at 73 °C on the basis of X-ray diffraction and DTA experiments. The form below 73 °C as well as the form in the temperature range from 73 to 164 °C are both trigonal with space group $P3_1$. Comparison of the structures at 23 and 99 °C shows that the phase transition is associated with displacements−reorientations of the almost planar NO_3 groups and a 90° flip of one-third of the NO_3 groups.

The variations in quadrupole coupling tensor elements and isotropic chemical shifts for $RbNO_3$ show no discontinuities over the studied temperature range, a fact that gives no evidence for a structural phase transition at about 73 °C. We expect that the unique variations in quadrupole coupling tensor elements may reflect effects from thermal expansion combined with the occurrence of reorientations−displacements of the NO_3 groups with variations in temperature. A continuous reorientation−displacement of the individual NO_3 groups with temperature will affect the Rb electric-field gradient tensors and the Rb atomic positions in a different manner. Thus, it seems plausible that such processes may account for the unique variations of the individual quadrupole tensor elements with temperature. Furthermore, increasing motional effects with increasing temperature, such as in-plane rotations of the NO_3 groups, may affect the electronic environments of the ^{87}Rb atoms and contribute to the unique temperature variations of the ^{87}Rb quadrupole tensors elements.

Conclusions

^{87}Rb quadrupole coupling parameters and isotropic chemical shifts have been presicely determined over a temperature range from about −100 to +165 °C for four inorganic rubidium salts from ^{87}Rb MAS NMR spectra of the central transition and ^{87}Rb MQMAS NMR spectra. The results demonstrate that these methods are valuable NMR spectroscopic tools for probing temperature variations of the local electronic environments of Rb nuclei. This may be utilized in studies of structural phase transitions and of motional effects associated with temperature variations. Furthermore, a comparison of our data for $RbClO_4$, Rb_2SO_4, and $RbNO_3$ with those reported in the literature from NMR spectra at ambient temperatures shows that minor discrepancies in these data partly reflect variations in the actual sample temperatures. Such variations may, for example, result from frictional heating caused by the sample spinning.

Our results demonstrate that the ^{87}Rb quadrupole coupling parameters and isotropic chemical shifts are highly temperature-dependent over the studied temperature range. Except for the Rb(2) site of Rb_2SO_4, the isotopic chemical shifts are observed to decrease linearly with increasing temperature with temperature coefficients in the range −0.014 to −0.036 ppm/°C. Linearly decreasing quadrupole coupling constants with increasing temperatures have been observed for $RbClO_4$, Rb_2SO_4, and the Rb(1) and Rb(3) sites of $RbNO_3$ with temperature coefficients in the range −1.6 to −7.0 kHz/°C. The linear relations between the principal elements of the quadrupole tensors for Rb_2SO_4 and temperature may be related to lattice dilatation and a linear increase of the lattice constants with increasing temperature. However, the more complex relations between the quadrupole tensor elements for $RbClO_4$ and $RbNO_3$ and temperature indicate that displacements−reorientations of the ClO_4^- and NO_3^- ions also contribute to the observed variations in ^{87}Rb quadrupole coupling parameters.

Acknowledgment. The use of the facilities at the Instrument Centre for Solid-State NMR Spectroscopy, University of Aarhus, sponsored by the Danish Research Councils (SNF and STVF), Teknologistyrelsen, Carlsbergfondet, and Direktør Ib Henriksens Fond, is acknowledged. We thank the Danish Natural Science Research Council (SNF) and Carlsbergforndet for financial support in the development of variable-temperature NMR equipment. M. Sc. Bjarke V. Schønwandt is acknowledged for help with some of the VT experiments.

References and Notes

(1) Cheng, J. T.; Edwards, J. C.; Ellis, P. D. *J. Phys. Chem.* **1990**, *94*, 553.
(2) Koons, J. M.; Hughes, E.; Cho, H. M.; Ellis, P. D. *J. Magn. Reson., Ser. A* **1995**, *114*, 12.
(3) Vosegaard, T.; Skibsted, J.; Bildsøe, H.; Jakobsen, H. J. *J. Magn. Reson., Ser. A* **1996**, *122*, 111.
(4) Vosegaard, T.; Skibsted, J.; Bildsøe, H.; Jakobsen, H. J. *J. Phys. Chem.* **1995**, *99*, 10731.
(5) Fernandez, C.; Amoureux, J. P.; Bodart, P.; Maijanen, A. *J. Magn. Reson., Ser. A* **1995**, *113*, 205.
(6) Medek, A.; Sachleben, J. R.; Beverwyk, P.; Frydman, L. *J. Chem. Phys.* **1996**, *104*, 5374.
(7) Shore, J. S.; Wang, S. H.; Taylor, R. E.; Bell, A. T.; Pines, A. *J. Chem. Phys.* **1996**, *105*, 9412.
(8) Baltisberger, J. H.; Gann, S. L.; Wooten, E. W.; Chang, T. H.; Mueller, K. T.; Pines, A. *J. Am. Chem. Soc.* **1992**, *114*, 7489.
(9) Grandinetti, P. J.; Baltisberger, J. H.; Llor, A.; Lee, Y. K.; Werner, U.; Eastman, M. A.; Pines, A. *J. Magn. Reson., Ser. A* **1993**, *103*, 72.
(10) Wang, S. H.; Xu, Z.; Baltisberger, J. H.; Bull, L. M.; Stebbins, J. F.; Pines, A. *Solid State Nucl. Magn. Reson.* **1997**, *8*, 1.
(11) Fernandez, C.; Amoureux, J. P. *Solid State Nucl. Magn. Reson.* **1996**, *5*, 315.
(12) Massiot, D.; Touzo, B.; Trumeau, D.; Coutures, J. P.; Virlet, J.; Florian, P.; Grandinetti, P. J. *Solid State Nucl. Magn. Reson.* **1996**, *6*, 73.
(13) Brown, S. P.; Wimperis, S. *J. Magn. Reson.* **1997**, *128*, 42.
(14) Bjørholm, T.; Jakobsen, H. J. *J. Magn. Reson.* **1989**, *84*, 204.
(15) Blinc, R.; Mali, M. *Phys. Rev.* **1969**, *179*, 552.
(16) Blinc, R.; O'Reilly, D. E.; Peterson, E. M. *Phys. Rev. B* **1970**, *1*, 1953.
(17) Blinc, R.; Južnič, S.; Rutar, V.; Seliger, J.; Zumer, S. *Phys. Rev. Lett.* **1980**, *44*, 609.
(18) Blinc, R.; Rutar, V.; Seliger, J.; Zumer, S.; Rasing, T.; Aleksandrova, I. P. *Solid State Commun.* **1980**, *34*, 895.
(19) Blinc, R.; Seliger, J.; Apih, T.; Dolinšek, J.; Fuith, A.; Schranz, W.; Warhanek, H. *Phys. Rev. B.* **1995**, *52*, 833.
(20) (a) Bhat, S. V.; Mahendroo, P. P. *Solid State Commun.* **1979**, *30*, 129. (b) Bhat, S. V.; Mahendroo, P. P.; Rigamonti, A. *Phys. Rev. B* **1979**, *20*, 1812.
(21) Borsa, F.; Benard, D. J.; Walker, W. C.; Baviera, A. *Phys. Rev. B* **1977**, *15*, 84.
(22) Kushida, T.; Benedek, G. B.; Bloembergen, N. *Phys. Rev.* **1956**, *104*, 1364.
(23) Honda, H.; Kenmotsu, M.; Ohki, H.; Ikeda, R.; Furukawa, Y. *Ber.*

Bunsen-Ges. Phys. Chem. **1995**, *99*, 1009.
(24) Ngai, L. H. *J. Phys. Chem. Solids* **1969**, *30*, 571.
(25) Hafner, S.; Nachtrieb, N. H. *J. Chem. Phys.* **1964**, *40*, 2891.
(26) (a) Guenther, B. D.; Hultsch, R. A. *J. Magn. Reson.* **1969**, *1*, 609. (b) Becker, K. D. *J. Chem. Phys.* **1978**, *68*, 3785.
(27) (a) Bielecki, A.; Burum, D. P. *J. Magn. Reson., Ser. A.* **1995**, *116*, 215. (b) Gorkom, L. C. M.; Hook, J. M.; Logan, M. B.; Hanna, J. V.; Wasylishen, R. E. *Magn. Reson. Chem.* **1995**, *33*, 791. (c) Mildner, T.; Ernst, H.; Freude, D. *Solid State Nucl. Magn. Reson.* **1995**, *5*, 269. (d) Neue, G.; Dybowski, C. *Solid State Nucl. Magn. Reson.* **1997**, *7*, 333.
(28) Pohl, J.; Pohl, D.; Adiwidjaja, G. *Acta Crystallogr.* **1992**, *B42*, 160.
(29) (a) Medek, A.; Harwood, J. S.; Frydman, L. *J. Am. Chem. Soc.* **1995**, *117*, 12779. (b) Wu, G.; Rovnyak, D.; Sun, B.; Griffin, R. G. *Chem. Phys. Lett.* **1996**, *249*, 210.
(30) Hanaya, M.; Harris, R. K. *J. Phys. Chem. A* **1997**, *101*, 6903.
(31) (a) Skibsted, J.; Bildsøe, H.; Jakobsen, H. J. *J. Magn. Reson.* **1991**, *92*, 669. (b) Skibsted, J.; Nielsen, N. C.; Bildsøe, H.; Jakobsen, H. J. *J. Magn. Reson.* **1991**, *95*, 88. (c) Skibsted, J.; Nielsen, N. C.; Bildsøe, H.; Jakobsen, H. J. *Chem. Phys. Lett.* **1992**, *188*, 405.
(32) Deshpande, V. T.; Sirdeshmukh, D. B. *Acta Crystallogr.* **1961**, *14*, 353.
(33) Tinkham, M. L.; Ellaboudy, A.; Dye, J. L.; Smidth, P. B. *J. Phys. Chem.* **1986**, *90*, 14.
(34) Frye, J. S.; Maciel, G. E. *J. Magn. Reson.* **1982**, *48*, 125.
(35) Granzin, J. *Z. Kristallogr.* **1988**, *184*, 157.
(36) Cohen, M. H.; Reif. F. *Solid State Phys.* **1957**, *5*, 321.
(37) Nord, A. G. *Acta Crystallogr.* **1974**, *B30*, 1640.
(38) (a) Shamsuzzoha, M.; Lucas, B. W. *Acta Crystallogr.* **1982**, *B38*, 2353. (b) Dean, C.; Hambley, T. W.; Snow, M. R. *Acta Crystallogr.* **1984**, *C40*, 1512.
(39) (a) Ahtee, M.; Hewat, A. W. *Phys. Status Solidi.* **1989**, *A58*, 525. (b) Shamsuzzoha, M.; Lucas, B. W. *Acta Crystallogr.* **1987**, *C43*, 385.
(40) Amoureux, J. P.; Fernandez, C.; Frydman, L. *Chem. Phys. Lett.* **1996**, *259*, 347.